Inverse Problems **16** (2000) 483–494. Printed in the UK PII: S0266-5611(00)04848-6

Imaging the solidification of molten metal by eddy currents: II

Minh H Pham†, Yingbo Hua† and Neil B Gray‡

† The Department of Electrical and Electronic Engineering, The University of Melbourne, Parkville, Victoria 3052, Australia
‡ The G K Williams Co-operative Research Centre for Extractive Metallurgy, Department of Chemical Engineering, The University of Melbourne, Parkville, Victoria 3052, Australia

E-mail: minhpham@ee.mu.oz.au and yhua@ee.mu.oz.au

Received 27 May 1999, in final form 20 December 1999

Abstract. This is the second part of two sister papers. The first paper developed an algorithm for imaging the solidification of molten metal inside a pipe where the conductivity of the metal inside the pipe was assumed to vary continuously (i.e., no clear boundary between the solid and the melt). Due to this nature, the algorithm shown in the first paper involves computationally expensive volume integrals. In this paper, the problem is slightly simplified where the molten metal and the solidification are assumed to have two distinct conductivities (i.e., there is a distinct boundary between the solid and the melt). This simplified problem allows us, in this paper, to develop a much faster imaging algorithm that involves a hybrid of volume and surface integrals. This hybrid technique provides great advantages over the surface or volume approaches alone.

1. Introduction

The object of interest is illustrated in figure 1. In this paper, we considered a two-dimensional problem by assuming that the pipe is penetrated with a two-dimensional magnetic field generated by infinitely long current line-sources, and that the solidification is the same along the pipe. (A three-dimensional model has been developed and will be reported in future papers.) When there is a distinct boundary between the solid metal and liquid metal, the geometry can be considered as three metal cylinders of different conductivities. The innermost cylinder has an unknown cross-section geometry (CSG). The outermost cylinder is circular. Our goal is to determine the CSG of the innermost cylinder based on a field measureable outside the object. Due to the high conductivity of metals, only a relatively low-frequency magnetic field can penetrate the object (of relatively small size) and generate a scattered electric field (outside the object) that contains useful information about the innermost cylinder. This scattered field has to be caused by the induced eddy currents inside the innermost cylinder.

Identification of the CSG of an infinitely long cylinder was considered by Colton and Kress [1]. Their method involves the conformal mapping taking the exterior of a disc onto the exterior boundary of the shape. Chiu and Kiang [2, 3] provided a computational approach to the problem by assuming either a perfectly conducting cylinder or a lossy cylinder with an approximated surface current density. Lin and Kiang [4] solved the problem for a dielectric cylinder in free space. The existing eddy-current inverse techniques [5, 6] solve very different problems. In this paper we deal with multilayered cylindrical background (figure 1). In this problem the computation of Green functions is critical. We will provide a set of the Green functions to take into account the multilayered geometry. [7] provides different approaches

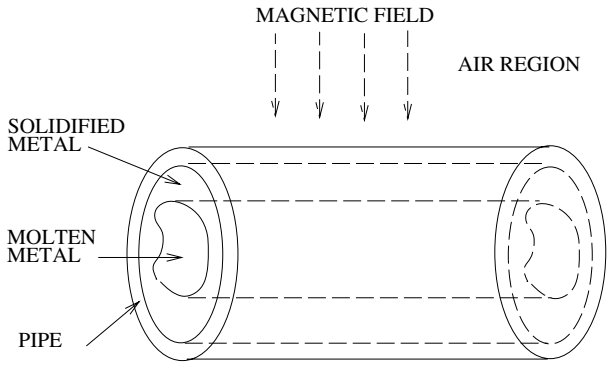

Figure 1. The geometry of the problem.

for solving the Green functions. Another source which deals with multilayered geometry is a book by Chew [8], although it does not deal explicitly with eddy-current problems.

This paper is organized as follows. Section 2 gives a further description of the problem, and formulates the problem quantitatively by partial differential equations. These partial differential equations are then transformed into integral equations using the Green function technique. A mathematical relationship between the scattered field and the shape of the cylinder is given through the set of integral equations. In section 3, an iterative algorithm for reconstructing the shape is described. The iterative procedure requires the computation of the electric field on the boundary of the innermost region at each iteration step. This electric field governed by a Fredholm integral equation of the second kind must be solved numerically because of the inherent complex geometry. A point-matching moments method is then employed to discretize the integral equation. Section 4 provides the simulation results to support our theory.

2. Modelling

2.1. Description of the problem

Figure 2 shows a cross-section of the geometry of the problem. The space is divided into four regions: region 0 (Ω_0) is the cross section of a homogeneous cylinder, region I (Ω_1) is the space exterior to the cylinder (in what follows, the cylinder refers to the innermost cylinder); region II is another circular layer and region III is the air outside the layered media. We denote the boundaries of the first three regions by Γ_0, Γ_1 and Γ_2, respectively. The boundary condition requires that the electric fields and their normal derivatives are continuous at the boundaries under the assumption that the relative permittivity and permeability in all regions are unity. The objective is to determine the curve Γ_0. The cylinder is penetrated with a time-varying magnetic field from line sources. This field creates eddy currents circulating in the object. The eddy currents in turn produce a scattered field which can be sensed in the exterior region (Ω_3). Based on the external measurements, the shape of the cylinder can be determined.

2.2. Integral equations for the electric field in region 0

The differential equation for the electric field in the region 0 is [9]

$$\nabla^2 E_0(\boldsymbol{r}) - k_0^2 E_0(\boldsymbol{r}) = 0, \qquad \forall \boldsymbol{r} \in \Omega_0 \tag{1}$$

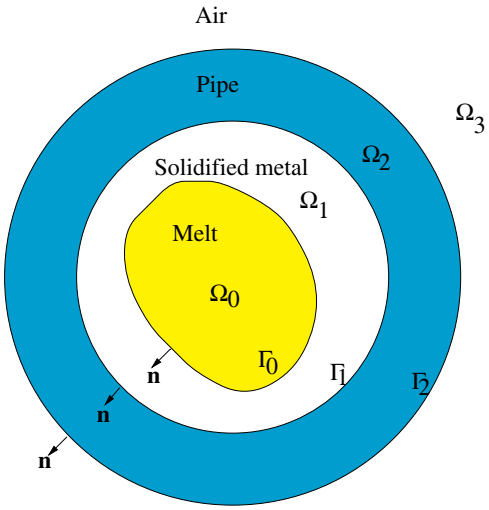

Figure 2. The geometry of the problem.

where $\boldsymbol{r} = (r, \phi)$, $k_0^2 = \mathrm{j}\omega\mu\sigma_0$, $\mathrm{j} = \sqrt{-1}$, ω the angular frequency, μ permeability, σ_0 the conductivity of the innermost cylinder and ∇^2 is the Laplace operator in polar coordinates. The relative permeability and permittivity are assumed to be unity in this paper. We define the Green function G_0 for the region 0 such that it satisfies the following relations:

$$\nabla^2 G_0(\boldsymbol{r}, \boldsymbol{r}') - k_0^2 G_0(\boldsymbol{r}, \boldsymbol{r}') = -\delta(\boldsymbol{r} - \boldsymbol{r}'), \qquad \forall \boldsymbol{r}, \qquad \boldsymbol{r}' \in R^2 \tag{2}$$

where R^2 is the whole two-dimensional space. Using the second Green identity, the integral equation for the electric field in region Ω_0 can be written in terms of the Green function G_0 as

$$c_0(\boldsymbol{r}) E_0(\boldsymbol{r}) = \int_{\Gamma_0} \left\{ G_0(\boldsymbol{r}, \boldsymbol{r}') \frac{\partial E_0}{\partial n'} - E_0(\boldsymbol{r}') \frac{\partial G_0}{\partial n'} \right\} \mathrm{d}\Gamma' \tag{3}$$

where $c_0(\boldsymbol{r}) = 1 : \boldsymbol{r} \in \Omega_0$; $\frac{1}{2} : \boldsymbol{r} \in \Gamma_0$; $0 : o/w$ and

$$G_0(\boldsymbol{r}, \boldsymbol{r}') = \frac{1}{2\pi} K_0(k_0 |\boldsymbol{r} - \boldsymbol{r}'|) \tag{4}$$

with K_0 being the modified Bessel function of the second kind [10]. Note that the field $E_0(\boldsymbol{r})$ in the whole domain Ω_0 is not determined from the integral equation (3) since the field and its normal derivative are unknowns on the boundary Γ_0. These two unknowns will be found by combining with another integral equation which is derived next.

2.3. Integral equation for electric field in region I

In the previous section, we set up an integral equation for the electric field in region 0. Although it is possible to do the same for regions II and III, this is unnecessary due to the circular geometry of regions II and III. We will now derive an integral equation for region I. In regions I, II and III, the electric fields are governed by

$$\nabla^2 E_u(\boldsymbol{r}) - k_u^2 E_u(\boldsymbol{r}) = \mathrm{j}\omega\mu J_u(\boldsymbol{r}), \qquad \forall \boldsymbol{r} \in \Omega_u \tag{5}$$

where $k_u^2 = \mathrm{j}\omega\mu\sigma_u$, $u = 1, 2, 3$, $\sigma_3 = 0$, $J_1 = 0$, $J_2 = 0$ and $J_3(\boldsymbol{r})$ is the externally applied current source. We define a set of Green's functions which satisfy

$$\begin{aligned} &\nabla^2 G_u^v(\boldsymbol{r}, \boldsymbol{r}') - k_u^v G_u^v(\boldsymbol{r}, \boldsymbol{r}') = -\delta(\boldsymbol{r} - \boldsymbol{r}'), \\ &\forall \boldsymbol{r} \in \bar{\Omega}_u, \qquad \boldsymbol{r}' \in \bar{\Omega}_v, \qquad u, v = 1, 2, 3 \end{aligned} \tag{6}$$

where $\bar{\Omega}_1 = \Omega_0 \cup \Omega_1$, $\bar{\Omega}_2 = \Omega_2$ and $\bar{\Omega}_3 = \Omega_3$. Applying the second Green's identity (with the convention that the unit normal vector always points from the inner region to the outer region) yields

$$c_1(\boldsymbol{r})E_1(\boldsymbol{r}) = \int_{\Gamma_1} \left\{ G_1^1(\boldsymbol{r},\boldsymbol{r}')\frac{\partial E_1}{\partial n'} - E_1(\boldsymbol{r}')\frac{\partial G_1^1}{\partial n'} \right\} \mathrm{d}\Gamma' - \int_{\Gamma_0} \left\{ G_1^1(\boldsymbol{r},\boldsymbol{r}')\frac{\partial E_1}{\partial n'} - E_1(\boldsymbol{r}')\frac{\partial G_1^1}{\partial n'} \right\} \mathrm{d}\Gamma' \tag{7}$$

where $c_1(\boldsymbol{r}) = 1 : \boldsymbol{r} \in \Omega_1; \frac{1}{2} : \boldsymbol{r} \in \Gamma_0 \cup \Gamma_1; 0 : o/w$,

$$\int_{\Gamma_1} \left\{ G_2^1(\boldsymbol{r},\boldsymbol{r}')\frac{\partial E_2}{\partial n'} - E_2(\boldsymbol{r}')\frac{\partial G_2^1}{\partial n'} \right\} \mathrm{d}\Gamma' = \int_{\Gamma_2} \left\{ G_2^1(\boldsymbol{r},\boldsymbol{r}')\frac{\partial E_2}{\partial n'} - E_2(\boldsymbol{r}')\frac{\partial G_2^1}{\partial n'} \right\} \mathrm{d}\Gamma', \quad \boldsymbol{r}' \in \Omega_2, \quad \boldsymbol{r} \in \bar{\Omega}_1 \tag{8}$$

$$\int_{\Omega_3} G_3^1(\boldsymbol{r},\boldsymbol{r}')\mathrm{j}\omega\mu J_3(\boldsymbol{r}')\,\mathrm{d}\Omega' = \int_{\Gamma_2} \left\{ G_3^1(\boldsymbol{r},\boldsymbol{r}')\frac{\partial E_3}{\partial n'} - E_3(\boldsymbol{r}')\frac{\partial G_3^1}{\partial n'} \right\} \mathrm{d}\Gamma', \quad \boldsymbol{r}' \in \Omega_3, \quad \boldsymbol{r} \in \bar{\Omega}_1. \tag{9}$$

Electric fields and their normal derivatives must be continuous on the boundaries. This is generally not requied for the Green functions. However, if we choose the Green functions in such a way that G_1^1, G_2^1, G_3^1 and their normal derivatives are continuous on Γ_1 and Γ_2, the equations (7)–(9) will be related to each other, and the six unknowns (E_1, $\partial E_1/\partial n$, E_2, $\partial E_2/\partial n$, E_3, $\partial E_3/\partial n$) on the boundaries will be reduced to only two. The integral equation (7) can now be written as

$$c_1(\boldsymbol{r})E_1(\boldsymbol{r}) = -\int_{\Omega_3} G_3^1(\boldsymbol{r},\boldsymbol{r}')\mathrm{j}\omega\mu J_3(\boldsymbol{r}')\,\mathrm{d}\Omega' - \int_{\Gamma_0} \left\{ G_1^1(\boldsymbol{r},\boldsymbol{r}')\frac{\partial E_1}{\partial n'} - E_1(\boldsymbol{r}')\frac{\partial G_1^1}{\partial n'} \right\} \mathrm{d}\Gamma'. \tag{10}$$

Equations (3) and (10) can be solved using the moments method [11, 12]. On the boundary Γ_0, we define

$$E_1(\boldsymbol{r}')|_{\boldsymbol{r}'\in\Gamma_0} = E_0(\boldsymbol{r}')|_{\boldsymbol{r}'\in\Gamma_0} \equiv M(\boldsymbol{r}') \tag{11}$$

$$\frac{\partial E_1}{\partial n'}|_{\boldsymbol{r}'\in\Gamma_0} = \frac{\partial E_0}{\partial n'}|_{\boldsymbol{r}'\in\Gamma_0} \equiv J(\boldsymbol{r}'). \tag{12}$$

On Γ_0, integral equations (3) and (10) become

$$\frac{M(\boldsymbol{r})}{2} - \int_{\Gamma_0} \left\{ J(\boldsymbol{r}')G_0(\boldsymbol{r},\boldsymbol{r}') - M(\boldsymbol{r}')\frac{\partial G_0}{\partial n'} \right\} \mathrm{d}\Gamma' = 0, \qquad \forall \boldsymbol{r} \in \Gamma_0 \tag{13}$$

$$\frac{M(\boldsymbol{r})}{2} + \int_{\Gamma_0} \left\{ J(\boldsymbol{r}')G_1^1(\boldsymbol{r},\boldsymbol{r}') - M(\boldsymbol{r}')\frac{\partial G_1^1}{\partial n'} \right\} \mathrm{d}\Gamma' = M_0(\boldsymbol{r}), \qquad \forall \boldsymbol{r} \in \Gamma_0 \tag{14}$$

where

$$M_0(\boldsymbol{r}) \equiv \mathrm{j}\omega\mu \int_{\Omega_3} G_3^1(\boldsymbol{r},\boldsymbol{r}')J_3(\boldsymbol{r}')\,\mathrm{d}\Omega', \qquad \forall \boldsymbol{r} \in \Gamma_0. \tag{15}$$

To solve for (13) and (14) we expand the functions J and M into series, i.e.,

$$M(\boldsymbol{r}) = \sum_{p=1}^{P} a_p \psi_p(\boldsymbol{r}), \qquad \forall \boldsymbol{r} \in \Gamma_0 \tag{16}$$

$$J(\boldsymbol{r}) = \sum_{p=1}^{P} b_p \chi_p(\boldsymbol{r}), \qquad \forall \boldsymbol{r} \in \Gamma_0 \tag{17}$$

where $\psi_p(\boldsymbol{r})$ and $\chi_p(\boldsymbol{r})$ are sets of independent basis functions for $M(\boldsymbol{r})$ and $J(\boldsymbol{r})$ respectively; a and b are unknown coefficients to be determined. Substituting (16) and (17) into (13) and (14) we obtain

$$\boldsymbol{h}_0^T(\boldsymbol{r})\boldsymbol{a} + \boldsymbol{g}_0^T(\boldsymbol{r})\boldsymbol{b} = 0 \tag{18}$$

$$\boldsymbol{h}_1^T(\boldsymbol{r})\boldsymbol{a} + \boldsymbol{g}_1^T(\boldsymbol{r})\boldsymbol{b} = M_0(\boldsymbol{r}) \tag{19}$$

where

$$\boldsymbol{a} = [a_1 \dots a_P]^T, \qquad \boldsymbol{b} = [b_1 \dots b_P]^T \tag{20}$$

$$\boldsymbol{h}_0(\boldsymbol{r}) = \left[\psi_1(\boldsymbol{r})/2 + \int_{\Gamma_0} \psi_p(\boldsymbol{r}')\frac{\partial G_0}{\partial n'}\,\mathrm{d}\Gamma' \dots \psi_P(\boldsymbol{r})/2 + \int_{\Gamma_0} \psi_P(\boldsymbol{r}')\frac{\partial G_0}{\partial n'}\,\mathrm{d}\Gamma'\right]^T \tag{21}$$

$$\boldsymbol{h}_1(\boldsymbol{r}) = \left[\psi_1(\boldsymbol{r})/2 - \int_{\Gamma_0} \psi_p(\boldsymbol{r}')\frac{\partial G_1^1}{\partial n'}\,\mathrm{d}\Gamma' \dots \psi_P(\boldsymbol{r})/2 - \int_{\Gamma_0} \psi_P(\boldsymbol{r}')\frac{\partial G_1^1}{\partial n'}\,\mathrm{d}\Gamma'\right]^T \tag{22}$$

$$\boldsymbol{g}_0(\boldsymbol{r}) = \left[-\int_{\Gamma_0} \chi_p(\boldsymbol{r}')G_0(\boldsymbol{r},\boldsymbol{r}')\,\mathrm{d}\Gamma' \dots - \int_{\Gamma_0} \chi_P(\boldsymbol{r}')G_0(\boldsymbol{r},\boldsymbol{r}')\,\mathrm{d}\Gamma'\right]^T \tag{23}$$

$$\boldsymbol{g}_1(\boldsymbol{r}) = \left[\int_{\Gamma_0} \chi_p(\boldsymbol{r}')G_1^1(\boldsymbol{r},\boldsymbol{r}')\,\mathrm{d}\Gamma' \dots \int_{\Gamma_0} \chi_P(\boldsymbol{r}')G_1^1(\boldsymbol{r},\boldsymbol{r}')\,\mathrm{d}\Gamma'\right]^T. \tag{24}$$

Sampling equations (18) and (19) at P points on the curve Γ_0 gives the following results:

$$\begin{bmatrix} \boldsymbol{h}_0^T(\boldsymbol{r}_1) \\ \vdots \\ \boldsymbol{h}_0^T(\boldsymbol{r}_P) \end{bmatrix}\boldsymbol{a} + \begin{bmatrix} \boldsymbol{g}_0^T(\boldsymbol{r}_1) \\ \vdots \\ \boldsymbol{g}_0^T(\boldsymbol{r}_P) \end{bmatrix}\boldsymbol{b} = \begin{bmatrix} 0 \\ \vdots \\ 0 \end{bmatrix} \tag{25}$$

$$\begin{bmatrix} \boldsymbol{h}_1^T(\boldsymbol{r}_{1+P}) \\ \vdots \\ \boldsymbol{h}_1^T(\boldsymbol{r}_{2P}) \end{bmatrix}\boldsymbol{a} + \begin{bmatrix} \boldsymbol{g}_1^T(\boldsymbol{r}_{1+P}) \\ \vdots \\ \boldsymbol{g}_1^T(\boldsymbol{r}_{2P}) \end{bmatrix}\boldsymbol{b} = \begin{bmatrix} M_0(\boldsymbol{r}_{1+P}) \\ \vdots \\ M_0(\boldsymbol{r}_{2P}) \end{bmatrix} \tag{26}$$

or

$$\boldsymbol{H}_0\boldsymbol{a} + \boldsymbol{G}_0\boldsymbol{b} = \boldsymbol{0} \tag{27}$$

$$\boldsymbol{H}_1\boldsymbol{a} + \boldsymbol{G}_1\boldsymbol{b} = \boldsymbol{M}_0. \tag{28}$$

All the a and b coefficients can be solved from (27) and (28). They are given by

$$\boldsymbol{a} = (\boldsymbol{H}_1 - \boldsymbol{G}_1\boldsymbol{G}_0^{-1}\boldsymbol{H}_0)^{-1}\boldsymbol{M}_0 \tag{29}$$

$$\boldsymbol{b} = (\boldsymbol{G}_1 - \boldsymbol{H}_1\boldsymbol{H}_0^{-1}\boldsymbol{G}_0)^{-1}\boldsymbol{M}_0. \tag{30}$$

It is interesting to observe what happens when the conductivities of regions 0 and I are the same ($k_0 = k_1$). We choose the Green function G_0 to be the same as G_1^1. Adding (13) and (14) gives $M(\boldsymbol{r}) = M_0(\boldsymbol{r})|_{\boldsymbol{r}\in\Gamma_0}$. For $\boldsymbol{r} \in \Omega_1$, $c_0(\boldsymbol{r}) = 0$ and from (3) and (10) we have $E_1(\boldsymbol{r}) = \int_{\Omega_3} G_3^1(\boldsymbol{r},\boldsymbol{r}')\mathrm{j}\omega\mu J_3(\boldsymbol{r}')\,\mathrm{d}\Omega'$. For $\boldsymbol{r} \in \Omega_0$, $c_1(\boldsymbol{r}) = 0$ and also from (3) and (10) we have $E_0(\boldsymbol{r}) = \int_{\Omega_3} G_3^1(\boldsymbol{r},\boldsymbol{r}')\mathrm{j}\omega\mu J_3(\boldsymbol{r}')\,\mathrm{d}\Omega'$. In other words, the solutions in the regions Ω_0 and Ω_1 are given by the same expression.

2.4. Integral equations for the scattered electric field in region III

Once the equivalent magnetic and electric current sources M and J are obtained, the electric field in region III can also be computed. The electric field in region III can be written in terms of the equivalent surface sources, M and J, on the curve Γ_0 if the Green functions G_u^3 values satisfy the same set of boundary conditions as the G_u^1 values. That is, the Green functions G_u^3

values and their normal derivatives are continuous on the boundaries. Following the same line of reasoning as in section 2.3, we obtain

$$c_3(\boldsymbol{r})E_3(\boldsymbol{r}) = E_i(\boldsymbol{r}) + \int_{\Gamma_0} \left\{ G_3^1(\boldsymbol{r}, \boldsymbol{r}')J(\boldsymbol{r}') - M(\boldsymbol{r}')\frac{\partial G_3^1}{\partial n'} \right\} \mathrm{d}\Gamma' \tag{31}$$

where $c_3(\boldsymbol{r}') = 1 : \boldsymbol{r}' \in \Omega_3;\ 1/2 : \boldsymbol{r}' \in \Gamma_0 \cup \Gamma_2;\ 0 : o/w$, and E_i is the incident field:

$$E_i(\boldsymbol{r}) = -\mathrm{j}\omega\mu \int_{\Omega_3} G_3^3(\boldsymbol{r}, \boldsymbol{r}')J_3(\boldsymbol{r}')\,\mathrm{d}\Omega'. \tag{32}$$

The scattered field is given by

$$E_s(\boldsymbol{r}) = \int_{\Gamma_0} \left\{ G_3^1(\boldsymbol{r}, \boldsymbol{r}')J(\boldsymbol{r}') - M(\boldsymbol{r}')\frac{\partial G_3^1}{\partial n'} \right\} \mathrm{d}\Gamma', \qquad \forall \boldsymbol{r} \in \Omega_3. \tag{33}$$

3. Inverse problem

Assume that the scattered field can be collected by a long rectangular solenoid [13]. The two arms of the solenoid are located at positions $\boldsymbol{r}$ and $\boldsymbol{r} - \Delta\boldsymbol{a}$, respectively. The voltage (per unit length) induced in the solenoid is then

$$V_s(\boldsymbol{r}) = \int_{\Gamma_0} \left\{ H_3^1(\boldsymbol{r}, \boldsymbol{r}')J(\boldsymbol{r}') - M(\boldsymbol{r}')\frac{\partial H_3^1}{\partial n'} \right\} \mathrm{d}\Gamma', \qquad \forall \boldsymbol{r} \in \Omega_3 \tag{34}$$

where $H_3^1(\boldsymbol{r}, \boldsymbol{r}') = G_3^1(\boldsymbol{r}, \boldsymbol{r}') - G_3^1(\boldsymbol{r} - \Delta\boldsymbol{a}, \boldsymbol{r}')$. Our reconstruction algorithm is an iterative process where each iteration consists of a forward part and an inverse part. In the forward part, the scattered field E_s is calculated using the previous estimate of Γ_0. This is achieved by first solving M, J using (13), (14) and then calculating V_s in (34). For the inverse part, a new estimate of Γ_0 is computed based on the error between the actual (measured) V_s and the previous estimate of V_s.

From our first paper in this series [13], we note that the scattered field can also be written as

$$V_s(\boldsymbol{r}) = (k_0^2 - k_1^2) \int_{\Omega_0} G_3^1(\boldsymbol{r}, \boldsymbol{r}')E_0(\boldsymbol{r})\,\mathrm{d}\Omega', \qquad \forall \boldsymbol{r} \in \Omega_3. \tag{35}$$

Equations (34) and (35) are equivalent, both of which will be used according to computational convenience. A smooth curve can be represented by a Fourier series

$$\Gamma_0 = \left\{ (\rho(\phi), \phi) : \rho(\phi) = \sum_{n=0}^{N} A(n)\cos(n\phi) + \sum_{n=1}^{N} B(n)\sin(n\phi), \phi \in [0, 2\pi] \right\} \tag{36}$$

where $A(n)$ and $B(n)$ are unknown coefficients to be determined. From (34), we define an error functional

$$U(\rho; \boldsymbol{r}) = V_s(\boldsymbol{r}) - \int_{\Gamma_0} \left\{ H_3^1(\boldsymbol{r}, \boldsymbol{r}')J(\boldsymbol{r}) - \frac{\partial H_3^1}{\partial n'}M(\boldsymbol{r}) \right\} \mathrm{d}\Gamma', \qquad \forall \boldsymbol{r} \in \Omega_3 \tag{37}$$

or

$$U(\rho; \boldsymbol{r}) = V_s(\boldsymbol{r}) - \int_0^{2\pi} \left\{ H_3^1(\boldsymbol{r}, \rho(\phi'), \phi')J(\rho(\phi'), \phi') - \frac{\partial H_3^1}{\partial n'}M(\rho(\phi'), \phi') \right\} \times \sqrt{\rho(\phi')^2 + \rho'(\phi')^2}\,\mathrm{d}\phi' \tag{38}$$

where $V_s(\boldsymbol{r})$ is the measurement obtained at position $\boldsymbol{r}$. If the measurements are taken at L different positions, we want to find such ρ values that minimize $\sum_{l=1}^{L} |U(\rho; \boldsymbol{r}_l)|^2$. To develop an iterative algorithm, we start with the first-order Taylor series expansion

$$|U(\rho + \delta\rho; \boldsymbol{r})|^2 \approx |U(\rho; \boldsymbol{r})|^2 + 2\mathrm{Re}\left[U^*(\rho; \boldsymbol{r})\frac{\mathrm{d}U(\rho; \boldsymbol{r})}{\mathrm{d}\rho}\delta\rho\right]. \tag{39}$$

From (38), the quantity $\frac{\mathrm{d}U(\rho;\boldsymbol{r})}{\mathrm{d}\rho}\delta\rho$ is given by

$$\begin{aligned}\frac{\mathrm{d}U(\rho; \boldsymbol{r})}{\mathrm{d}\rho}\delta\rho = &-\int_0^{2\pi} \frac{\partial}{\partial\rho}\left[H_3^1(\boldsymbol{r}, \rho(\phi'), \phi')J(\rho(\phi'), \phi')\sqrt{\rho(\phi')^2 + \rho'(\phi')^2}\right]\delta\rho(\phi')\,\mathrm{d}\phi' \\ &+\int_0^{2\pi} \frac{\partial}{\partial\rho}\left[\frac{\partial H_3^1}{\partial n'}M(\rho(\phi'), \phi')\sqrt{\rho(\phi')^2 + \rho'(\phi')^2}\right]\delta\rho(\phi')\,\mathrm{d}\phi'.\end{aligned} \tag{40}$$

In the spirit of the Born approximation, (40) becomes

$$\begin{aligned}\frac{\mathrm{d}U(\rho; \boldsymbol{r})}{\mathrm{d}\rho}\delta\rho = &-\int_0^{2\pi} \frac{\partial}{\partial\rho}\left[H_3^1(\boldsymbol{r}, \rho(\phi'), \phi')\sqrt{\rho(\phi')^2 + \rho'(\phi')^2}\right]J(\rho(\phi'), \phi')\delta\rho(\phi')\,\mathrm{d}\phi' \\ &+\int_0^{2\pi} \frac{\partial}{\partial\rho}\left[\frac{\partial H_3^1}{\partial n'}\sqrt{\rho(\phi')^2 + \rho'(\phi')^2}\right]M(\rho(\phi'), \phi')\delta\rho(\phi')\,\mathrm{d}\phi'.\end{aligned} \tag{41}$$

However, a much simpler expression can be obtained by using the volume integral equation for the scattered field. Using (35), the functional $U(\rho; \boldsymbol{r})$ can also be written as

$$U(\rho; \boldsymbol{r}) = V_s(\boldsymbol{r}) - (k_0^2 - k_1^2)\int_0^{2\pi}\int_0^{\rho(\phi')} H_3^1(\boldsymbol{r}, r', \phi')E_0(r', \phi')r'\,\mathrm{d}r'\,\mathrm{d}\phi'. \tag{42}$$

The variation with respect to ρ is then

$$\frac{\mathrm{d}U(\rho; \boldsymbol{r})}{\mathrm{d}\rho}\delta\rho = -(k_0^2 - k_1^2)\int_0^{2\pi} H_3^1(\boldsymbol{r}, \rho(\phi'), \phi')M(\rho(\phi'), \phi')\rho(\phi')\delta\rho(\phi')\,\mathrm{d}\phi'. \tag{43}$$

We see that (41) and (43) are equivalent. However, the latter is much simpler. Using the volume integral equation for the scattered field defined in (35), there is no need to differentiate the Green function and the integral is less computationally demanding. Now, equation (39) can be written as

$$|U(\rho + \delta\rho; \boldsymbol{r})|^2 \approx |U(\rho; \boldsymbol{r})|^2 + \sum_{n=0}^{N}\delta A(n)C(n; \boldsymbol{r}) + \sum_{n=1}^{N}\delta B(n)S(n; \boldsymbol{r}) \tag{44}$$

$$|U(\rho + \delta\rho; \boldsymbol{r})|^2 \approx |U(\rho; \boldsymbol{r})|^2 + \boldsymbol{p}^T(\boldsymbol{r})\delta\boldsymbol{q} \tag{45}$$

where

$$\begin{aligned}C(n; \boldsymbol{r}) = -2\mathrm{Re}\Bigg[&(k_0^2 - k_1^2)U^*(\rho; \boldsymbol{r})\int_0^{2\pi} H_3^1(\boldsymbol{r}, \rho(\phi'), \phi')M(\rho(\phi'), \phi') \\ &\times \cos(n\phi')\rho(\phi')\,\mathrm{d}\phi'\Bigg]\end{aligned} \tag{46}$$

$$\begin{aligned}S(n; \boldsymbol{r}) = -2\mathrm{Re}\Bigg[&(k_0^2 - k_1^2)U^*(\rho; \boldsymbol{r})\int_0^{2\pi} H_3^1(\boldsymbol{r}, \rho(\phi'), \phi')M(\rho(\phi'), \phi') \\ &\times \sin(n\phi')\rho(\phi')\,\mathrm{d}\phi'\Bigg]\end{aligned} \tag{47}$$

$$\boldsymbol{p}(\boldsymbol{r}) = [C(0, \boldsymbol{r}) \ldots C(N, \boldsymbol{r})S(1, \boldsymbol{r}) \ldots S(N, \boldsymbol{r})]^T \tag{48}$$

$$\boldsymbol{q} = [A(0) \ldots A(N)B(1) \ldots B(N)]^T. \tag{49}$$

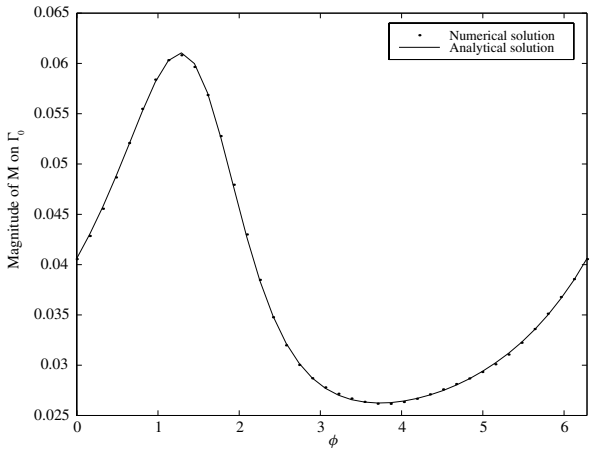

Figure 3. The magnitude of M on Γ_0.

Given the measurements taken at L different angles, we stack equation (45) as follows:

$$\begin{bmatrix} |U(\rho+\delta\rho;\boldsymbol{r}_1)|^2 \\ \vdots \\ |U(\rho+\delta\rho;\boldsymbol{r}_L)|^2 \end{bmatrix} = \begin{bmatrix} |U(\rho;\boldsymbol{r}_1)|^2 \\ \vdots \\ |U(\rho;\boldsymbol{r}_L)|^2 \end{bmatrix} + \begin{bmatrix} \boldsymbol{p}^T(\boldsymbol{r}_1) \\ \vdots \\ \boldsymbol{p}^T(\boldsymbol{r}_L) \end{bmatrix} \delta\boldsymbol{q} \tag{50}$$

or in vector form

$$\boldsymbol{e} = \boldsymbol{u} + \boldsymbol{P}\delta\boldsymbol{q}. \tag{51}$$

Let the shape function ρ after the mth iteration be ρ_m. It is then updated by finding an increment $\delta\rho_m$ such that $\sum_{l=1}^{L} |U(\rho_m+\delta\rho_m;\boldsymbol{r}_l)|^2$ is minimized. This can be done via the increment $\delta\boldsymbol{q}_m$:

$$\delta\boldsymbol{q}_m = \arg\min_{\boldsymbol{x}} \|\boldsymbol{u}_m + \boldsymbol{P}_m\boldsymbol{x}\|. \tag{52}$$

Note that the updated boundary at the mth iteration may be extended beyond the boundary Γ_1, which is not desirable. In such a case, the new estimate will be

$$\rho_{0,m+1} = \max\{\rho_{0,m} + \delta\rho_{0,m}, r_1\}. \tag{53}$$

In general, it is not possible to find $\delta\boldsymbol{q}_m$ by minimizing the norm $\|\boldsymbol{u}_m + \boldsymbol{P}_m\boldsymbol{x}\|$. This is due to the ill-conditioning of the matrix $\boldsymbol{P}$. When noise exists in measurements, the increment $\delta\boldsymbol{q}$ may be very large. Regularization can reduce this effect. Many different techniques such as singular value decomposition, least squares etc [14] have been used. In our experience, the constrained optimization procedure [14] is the most stable.

4. Simulation

Example 1. To compute the quantities J and M, we use the trigonometric series

$$J(\phi) = \sum_{p=0}^{8} a_p \cos^p(\phi) + \sum_{p=1}^{8} b_p \sin(\phi)\cos^{p-1}(\phi) \tag{54}$$

where a_p and b_p are to be determined. The above series is equivalent to a Fourier series. However, its basis functions are not at all oscillatory and therefore generic quadrature subroutines can be applied to it. The expression for J is similar. The numerical solution

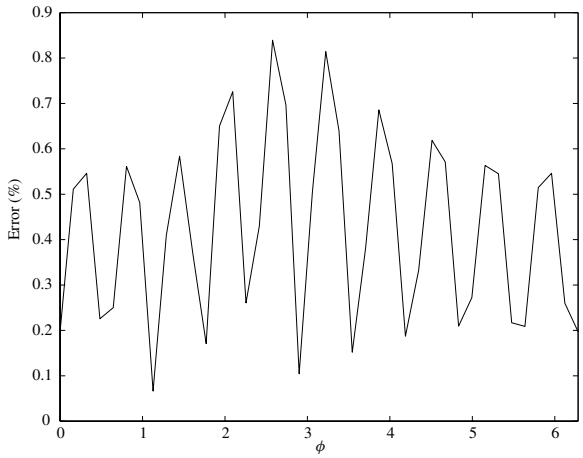

Figure 4. The error of the numerical solution.

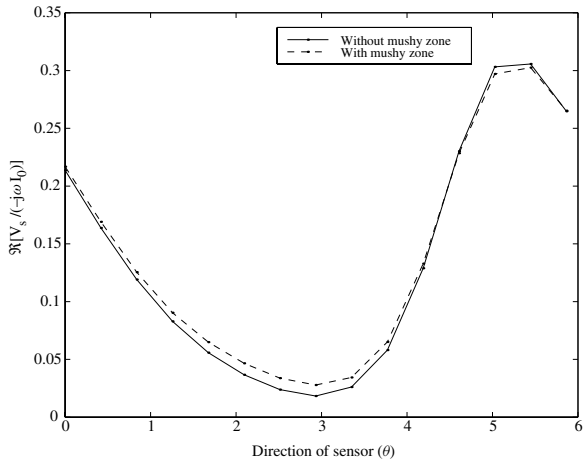

Figure 5. Real part of $\frac{V_s}{-j\omega I_0}$ versus the direction of solenoid (θ): with and without the mushy zone.

for M is shown in figure 3. The numerical solution is very accurate with less than 0.9% error compared with the analytical solution (figure 4).

Example 2. Comparisons between the volume integral approaches [13] and hybrid integral approach of this paper is shown in figures 5 and 6. It can be seen that the effect of the mushy zone is not very significant. In the simulation, we use the data generated by the volume integral approach (where the mushy zone is assumed to exist) as the measurements for the reconstruction.

The relative root mean square error (RMSE) of the estimate at the kth iteration is given by

$$\mathrm{RMSE}_\rho = \sqrt{\frac{\sum_{n=0}^{N}(A_k - A_{\mathrm{actual}})^2(n) + \sum_{n=1}^{N}(B_k - B_{\mathrm{actual}})^2(n)}{\sum_{n=0}^{N} A_{\mathrm{actual}}^2(n) + \sum_{n=1}^{N} B_{\mathrm{actual}}^2(n)}}. \tag{55}$$

Let the initial shape function be a circle. Figure 7 shows the convergence of the shape at the

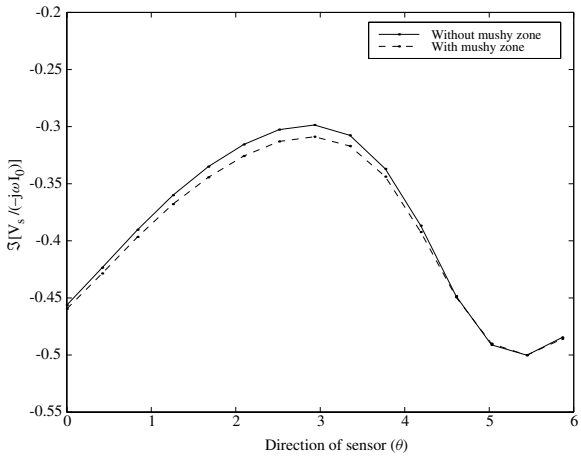

Figure 6. Imaginary part of $\frac{V_s}{-j\omega I_0}$ versus the direction of the solenoid (θ): with and without the mushy zone.

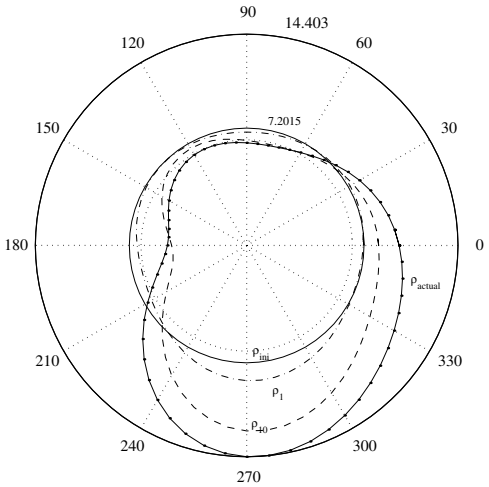

Figure 7. Actual shape, first and tenth estimate of ρ.

first and tenth iterations. Each iteration takes about 10 s CPU time. The estimate ρ converges close to the actual ρ value after 50 iterations. Hence the effect of the mushy zone is not very significant in determining the shape of the solidification.

5. Conclusion

In this paper, we developed a hybrid surface-volume eddy-current inversion technique for reconstructing the shape of solidification. This hybrid technique involves mostly surface integrals and hence is much more efficient numerically than the volume integral-based technique. In most practical applications, the assumption of no mushy zone causes only a small change in the measurable scattered field as could be seen in our simulations. Hence the hybrid surface-volume integral approach is justified.

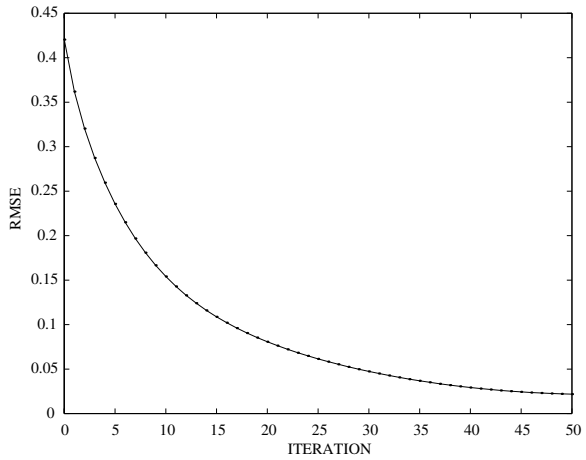

Figure 8. Relative error versus the number of iterations.

Acknowledgments

This work has been supported by the Australian Cooperative Research Centre for Sensor Signal and Information Processing (CSSIP) and the G K Williams Co-operative Research Centre for Extractive Metallurgy.

Appendix

The most time consuming part of the moments method is to evaluate the matrix elements. We first consider the elements of the matrix $\boldsymbol{G_0}$:

$$(\boldsymbol{G_0})_{ij} = -\int_{\Gamma_0} \chi_j(\boldsymbol{r}')G_0(\boldsymbol{r}_i, \boldsymbol{r}')\,\mathrm{d}\Gamma', \qquad i, j = 1, \ldots, P. \tag{56}$$

In polar coordinates, the matrix element $(\boldsymbol{G_0})_{ij}$ is written as

$$(\boldsymbol{G_0})_{ij} = \frac{-1}{2\pi}\int_0^{2\pi} \chi_j(\phi')K_0\left(k_0\sqrt{\rho(\phi_i)^2 + \rho(\phi')^2 - 2\rho(\phi_i)\rho(\phi')\cos(\phi_i - \phi')}\right) \times\sqrt{\rho(\phi')^2 + \rho'(\phi')^2}\,\mathrm{d}\phi' \tag{57}$$

where $\rho'(\phi)$ is the derivative of $\rho(\phi)$ with respect to ϕ. Numerical integration of (57) is difficult since the integrand is singular when $\phi' = \phi_i$. However, the singularity is weak and can be supressed by the following transformation technique. We divide the interval of the integration into two intervals: $[0, \phi_i)$ and $(\phi_i, 2\pi]$. Then, (57) can be transformed into

$$\begin{aligned}(\boldsymbol{G_0})_{ij} = {} & \frac{-1}{2\pi}\int_0^1 \chi_j(\phi'(\eta))K_0\left(k_0\sqrt{\rho(\phi_i)^2 + \rho(\phi')^2 - 2\rho(\phi_i)\rho(\phi'(\eta))\cos(\phi_i - \phi'(\eta))}\right) \\ & \times\sqrt{\rho(\phi'(\eta))^2 + \rho'(\phi'(\eta))^2}2\phi_i(1-\eta)\,\mathrm{d}\eta - \frac{1}{2\pi}\int_0^1 \chi_j(\phi'(\eta))K_0 \\ & \times\left(k_0\sqrt{\rho(\phi_i)^2 + \rho(\phi')^2 - 2\rho(\phi_i)\rho(\phi'(\eta))\cos(\phi_i - \phi'(\eta))}\right) \\ & \times\sqrt{\rho(\phi'(\eta))^2 + \rho'(\phi'(\eta))^2}2(2\pi - \phi_i)(1-\eta)\,\mathrm{d}\eta \end{aligned} \tag{58}$$

where $\phi' = \phi_i\eta(2-\eta)$ and $\phi' = 2\pi - (2\pi - \phi_i)\eta(2-\eta)$ in the first and second integrals of (58) respectively. It can be seen that the singularities have been suppressed at $\eta = 1$. Next, we consider the matrix elements of $\boldsymbol{H}_0$:

$$(\boldsymbol{H}_0)_{ij} = \frac{\psi_j(\boldsymbol{r}_i)}{2} - \int_{\Gamma_0} \psi_j(\boldsymbol{r}') \frac{\partial G_0(\boldsymbol{r}_i, \boldsymbol{r}')}{\partial n'} \,\mathrm{d}\Gamma' \tag{59}$$

where the expression of the normal derivative $\partial G_0/\partial n$ is given by

$$\begin{aligned}\frac{\partial G_0(\boldsymbol{r}_i, \boldsymbol{r})}{\partial n} = \frac{-k_0}{2\pi} & \frac{K_1\left(k_0\sqrt{\rho(\phi_i)^2 + \rho(\phi)^2 - 2\rho(\phi_i)\rho(\phi)\cos(\phi_i - \phi)}\right)}{\sqrt{\rho(\phi)^2 + \rho'(\phi)^2}\sqrt{\rho(\phi_i)^2 + \rho(\phi)^2 - 2\rho(\phi_i)\rho(\phi)\cos(\phi_i - \phi)}} \\ & \times(\rho(\phi)^2 - \rho(\phi_i)\rho(\phi)\cos(\phi_i - \phi) - \rho(\phi_i)\rho'(\phi)\sin(\phi_i - \phi)).\end{aligned} \tag{60}$$

The matrix element $(\boldsymbol{H}_0)_{ij}$ becomes

$$\begin{aligned}(\boldsymbol{H}_0)_{ij} = \frac{\psi_j(\boldsymbol{r}_i)}{2} + \frac{k_0}{2\pi}\int_0^{2\pi} & \psi_j(\phi') \\ & \times \frac{K_1\left(k_0\sqrt{\rho(\phi_i)^2 + \rho(\phi')^2 - 2\rho(\phi_i)\rho(\phi')\cos(\phi_i - \phi')}\right)}{\sqrt{\rho(\phi_i)^2 + \rho(\phi')^2 - 2\rho(\phi_i)\rho(\phi')\cos(\phi_i - \phi')}} \\ & \times(\rho(\phi')^2 - \rho(\phi_i)\rho(\phi')\cos(\phi_i - \phi') - \rho(\phi_i)\rho'(\phi')\sin(\phi_i - \phi'))\,\mathrm{d}\phi'.\end{aligned} \tag{61}$$

As $\phi' \to \phi_i$, the integrand in (61) is:

$$\begin{aligned}\lim_{\phi\to\phi_i} & \frac{\partial G_0(\boldsymbol{r}_i, \boldsymbol{r})}{\partial n} \\ & = \frac{-1}{2\pi}\lim_{\phi\to\phi_i} \frac{(\rho(\phi)^2 - \rho(\phi_i)\rho(\phi)\cos(\phi_i - \phi) - \rho(\phi_i)\rho'(\phi)\sin(\phi_i - \phi))}{\rho(\phi_i)^2 + \rho(\phi)^2 - 2\rho(\phi_i)\rho(\phi)\cos(\phi_i - \phi)}.\end{aligned} \tag{62}$$

At $\phi' = \phi_i$, the numerator and denominator approach zero and the limit may be infinite. We can apply the same transformations as before to eliminate the singularity. Elements of other matrices are evaluated in a similar manner.

References

[1] Colton D and Kress R 1992 *Inverse Acoustic and Electromagnetic Scattering Theory* (New York: Springer)

[2] Chiu C C and Kiang Y W 1991 Electromagnetic imaging for an imperfectly conducting cylinder *IEEE Trans. Microw. Theory Tech.* **39** 1632–9

[3] Chiu C C and Kiang Y W 1991 Inverse scattering of a buried conducting cylinder *Inverse Problems* **7** 187–202

[4] Lin H T and Kiang Y W 1994 Microwave imaging for a dielectric cylinder *IEEE Trans. Microw. Theory Tech.* **42** 1572–9

[5] Rose J H and Nair S M 1991 Exact recovery of the DC electrical conductivity of a layered solid *Inverse Problems* **7** L31–6

[6] Wismer M G and Ludwig R A 1992 Hybrid finite element/method of moment formulation for single frequency eddy-current inversion *IEEE Trans. Magn.* **28** 1843–9

[7] Minh H P 1997 Imaging the solidification of molten metal by eddy current *Melbourne University Annual Report*

[8] Chew W C 1990 *Waves and Fields in Inhomogeneous Media* (New York: Van Nostrand-Reinhold)

[9] Stratton J A 1941 *Electromagnetic Theory* (New York: McGraw-Hill)

[10] Abramowitz M and Stegun I A 1970 *Handbook of Mathematical Functions, with Formulae, Graphs, and Mathematical Tables* (New York: Dover)

[11] Harrington R F 1967 Matrix methods for field problems *Proc. IEEE* **55** 136–49

[12] Harrington R F 1968 *Field Computation by Moment Method* (New York: Macmillan)

[13] Minh H P, Hua Y and Gray B N 2000 Imaging the solidification of molten metal by eddy currents: I *Inverse Problems* submitted

[14] Golub G H and van Loan C F 1983 *Matrix Computation* (Oxford: North Oxford Academic)